SPEKTRA: Jurnal Fisika dan Aplikasinya
Volume 11, Issue 1, April 2026
Homepage: doi.org/10.21009/SPEKTRA

DOI: doi.org/10.21009/SPEKTRA.111.02

Pre-selection of Globular Clusters for Detecting Intermediate-Mass Black Holes via Microlensing

Fatimah Zahra[1,*], Anton Timur Jaelani[2,3,4]

[1]*Astronomy Master Program, FMIPA, Institut Teknologi Bandung, Jl. Ganesa 10, Bandung 40132, Indonesia*
[2]*Astronomy Research Group,, FMIPA, Institut Teknologi Bandung, Jl. Ganesa 10, Bandung 40132, Indonesia*
[3]*U-CoE AI-VLB, Institut Teknologi Bandung, Jl. Ganesa 10, Bandung 40132, Indonesia*
[4]*University center of Excellence for Space Science, Technology and Innovation, Institut Teknologi Bandung, Jl. Ganesa 10, Bandung 40132, Indonesia*

*Corresponding Author Email: fatzea@gmail.com

Received: 15 August 2025
Revised: 5 April 2025
Accepted: 30 April 2026
Online: 30 April 2026
Published: 30 April 2026

SPEKTRA: Jurnal Fisika dan Aplikasinya
p-ISSN: 2541-3384
e-ISSN: 2541-3392

ABSTRACT

Intermediate-mass black holes (IMBHs) are the key to understanding the formation of supermassive black holes (SMBHs) that are typically found in centers of massive galaxies. In general definition, IMBHs are black holes masses ranging from $10^2\ M_\odot$ to $10^5\ M_\odot$. Black hole seeding theory suggests that IMBHs formed at high redshifts ($z \geq 0$) through gravitational collapse of Population III stars, direct collapse of protogalaxy clouds, or stellar collisions inside high-density clusters. These IMBHs evolve into SMBHs through accretion and mergers. However, not all of these IMBHs are successful in forming SMBHs. Those that fail are hypothesized to be observable in the local universe, particularly in globular clusters and dwarf galaxies. IMBHs have yet to be definitively detected, however several strong candidates have been located in the cores of globular clusters. This study describes the preliminary selection stage of globular cluster candidates with the aim to look further into the possibility of detecting IMBHs via microlensing. The selection process was based on several physical properties of the globular clusters including mass, metallicity, and central velocity dispersion. Since background star density strongly affects microlensing detection probability, we restricted the sample to clusters located in the direction of the Galactic center. We utilized Gaia DR3 data to estimate background star density for selected globular clusters using proper motion filtering and Theil-Sen regression method. These estimates provide the foundation for further subsequent simulations of microlensing detection probabilities associated with central IMBHs.

Keywords: intermediate-mass black hole, globular cluster, microlensing, Gaia DR3, background star density

INTRODUCTION

Existence of black holes with masses $M \leq 100M_{\odot}$ and $M \geq 10^5\ M_{\odot}$ has been confirmed through various types of observations [1]. Stellar-mass black holes, black holes with masses $M \leq 100M_{\odot}$, are defined as the type of black holes formed through gravitational core collapse of massive stars. These black holes have been detected via observations of X-ray binary systems, gravitational waves, and gravitational microlensing events [2-4]. On the other hand, black holes with $M \geq 10^5\ M_{\odot}$ are known as supermassive black holes (SMBHs) and are commonly found at the center of massive galaxies. The SMBH at the center of Milky Way has been indirectly detected through the motion of surrounding hypervelocity stars [5] and through the detection of SMBH shadow in radio signal by the Event Horizon Telescope [6], while SMBHs in other massive galaxies can be identified through the presence of accretion disk called Active Galactic Nuclei features [7].

Although it is common to find SMBHs across the universe [8], the formation process of this type of black hole remains uncertain. Several theoretical models have been proposed to explain their origin: (i) SMBHs are formed from primordial gravitational potentials in the early universe, with dark matter acting as catalyst in their formation [9]; (ii) it is also possible that SMBHs are formed through extreme intensity of mergers stellar-mass black holes [10]; and lastly, (iii) SMBHs grow from 'seed' black holes within the range of missing mass link, $10^2\ M_{\odot} \leq M \leq 10^5\ M_{\odot}$, through a combination of mergers and accretion [1, 11-12]. This seeding scenario introduces a new type of black holes, the intermediate-mass black holes (IMBHs) [1].

Currently, the black hole seeding theory is one of the most favored models for explaining the abundance of SMBHs [13-14]. However, validating this theory requires observational confirmation of IMBHs, which up to this date has not been definitively detected although there are some strong candidates [13, 15]. According to the black hole seeding theory, IMBHs are expected to have formed at the dawn of the universe, at $z \geq 10$, in dense stellar clusters or near the center of its host galaxies. Therefore, the ideal strategy to detect these primordial IMBHs involves targeting high-redshift galaxies, $z \geq 7$, where many IMBHs may still exist prior to their growth into SMBHs. However, since IMBHs are 'dark' objects, such observations remain challenging with current technological capabilities [3].

However, not all IMBHs are predicted to have successfully evolved into SMBHs. A 'residual' population of IMBHs may be ejected from the centers of protogalaxies due to extreme gravitational interaction during merger events. Based on this, the search of IMBHs can be focused within the local universe, particularly in $z \geq 2.4$ [16]. In the Milky Way, these types of IMBHs are expected to be lying at the center of massive globular clusters (GCs). Based on the mass-velocity dispersion relation ($M - \sigma$) IMBHs are expected to reside in clusters with central velocity dispersions in the range $10 \leq \sigma \leq 20\ \mathrm{km\ s^{-1}}$, making GCs more likely to host IMBHs than open cluster [10, 17]. Furthermore, GCs generally have comparable ages with their host galaxies. This suggests that during the epoch of galaxy formation, seed IMBHs for the early growth of SMBHs may have transferred through GCs to the center of galaxies [10].

One of the current strongest candidate of IMBHs in the Milky Way is located in the center of ω Centauri. This IMBHs was identified through kinematic studies based on photometric and astrometric data [13]. However, other studies have challenged this finding, arguing that the presence of an IMBH at the center of ω Centauri remains unconfirmed due to discrepancies in stellar velocity measurements obtained using spectroscopic data [15].

Based on Einstein's general relativity, a sufficiently massive object warps surrounding spacetime, causing the trajectories of passing light rays to bend along curved paths [4, 16]. This gravitational lensing effect causes an apparent shift of the background source observed position relative to its true position, with the massive foreground object acting as the "lens". Gravitational microlensing refers to this phenomenon caused by relatively less-massive objects such as stars, planets, or in this case, IMBHs. In typical microlensing events, the apparent positional shift of the background source is too small to be directly resolved. Instead, the lensing effects can be detected as a transient magnification or sudden rise of the source brightness, producing the unique pattern of microlensing light curve. Through detected microlensing events, the mass and distance of the lens object can be directly constrained from the property of this magnification signal, providing an unambiguous method for IMBH detection [10, 18].

Previous studies have established microlensing as a promising method for IMBH detection, particularly in dense stellar fields such as in GCs in the central region of the Milky Way [10, 18]. Based on the Monte Carlo simulations done in the study, photometric microlensing by a central IMBH is intrinsically rare, but the associated astrometric signal caused by it is long-lived and measurable [10]. This framework was subsequently applied to archival Hubble Space Telescope (HST) data for NGC 6656 (M22), which yields no definitive detection that highlighted observational limitations for this method [18]. More recently, the work in [19] extended microlensing searches to quasars, demonstrating that existence of a central IMBHs in GCs can be constrained through long-term, quasi-linear variability that is distinguishable from the stochastic variability of quasars through its coherent multiwavelength behaviour.

In this work, we carry the pre-selection step for GCs following an approach motivated by [10], which built upon several earlier studies and defines a set of observational criteria for identifying GCs target for IMBH microlensing searches. While [10] relied on HST archival data and focused on observational constraints such as extinction, horizontal branch magnitude, and surface brightness profiles, we adopt a different strategy. Specifically, we replace these observational criteria by physical properties of GCs such as mass, extinction, and central velocity dispersion. These criteria are guided based on recent studies [20-21], which outline the physical conditions under which a GC is likely to host a central IMBHs.

The GCs are pre-selected based on their location. We consider only those located toward the Galactic center, where the high density of background stars enhances the probability of microlensing detection. Accordingly, we also estimate the background star density in each GC field to assess its suitability for microlensing searches.

MICROLENSING

In this section, we followed general description of gravitational (micro)lensing from [23-24]. A gravitational microlensing event involves a foreground massive object acting as a lens and a background light source. For the lensing effect to be observable, the observer, lens, and source must align along the same line of sight. When microlensing events occur within the galactic range (inside the Milky Way), the position of both lens and source will change over time. The time-dependent angular separation between lens and source, Φ, can be expressed its normalization to the angular radius of the lens's gravitational influence, Einstein ring radius, such as $u = \frac{\Phi}{\theta_E}$, given

$$\theta_E = \sqrt{\frac{4GM}{c^2}\frac{(D_S - D_L)}{D_S D_L}}, \tag{1}$$

where D_S and D_L are distances of observer to the source and observer to the lens, respectively. Microlensing is a transient phenomenon, meaning it typically occurs only once for a given source-lens pair, due to the relative motion of the lens and source. Thus, one if the key parameters in a microlensing event is the Einstein timescale, t_E, defined as

$$t_E = \frac{\theta_E}{\mu_{LS}}, \tag{2}$$

where μ_{LS} is the relative proper motion between lens and source. When the microlensing occurs, light rays from the source are deflected, giving the effect of magnification, which can be detected photometricly by analyzing the source light curve. A point source like star is magnified by a factor

$$A = \frac{u^2 + 2}{u\sqrt{u^2 + 4}}, \tag{3}$$

where A is changing overtime. The apparent position of the source also appears to change with time, and can be detected astrometricly. This apparent displacement of the source's centroid position, $\delta(u)$ is given by

$$\delta(u) = \frac{u}{u^2 + 2}\theta_E, \tag{4}$$

which have parallel and perpendicular components to the source-lens relative motion, $\delta_\parallel$ and $\delta_\perp$, that can be expressed as

$$\delta_\parallel = \frac{p}{u_0^2 + p^2 + 2}\theta_E, \qquad \delta_\perp = \frac{u_0}{u_0^2 + p^2 + 2}\theta_E, \tag{5}$$

where u_0 is the impact parameter, or the source closest angular separation from the lens, and p is the normalized time of observation to the Einstein timescale, expressed as

$$p \equiv \frac{t - t_0}{t_E}, \tag{6}$$

where t_0 is the time when the source reached u_0, or the time when the microlensing effect reached its peak.

For an IMBH residing at the center of a Galactic GC, we adopt a representative lens distance of $D_L = 4$ kpc and a background source star located in the galactic bulge at $D_S = 8.5$ kpc. Under these assumptions, the angular Einstein radius for an IMBH with mass $10^2 M_\odot$ is approximately $\theta_E \sim 10$ milliarcseconds, increasing to $\theta_E \sim 100$ milliarcseconds for an IMBH with mass of $10^5 M_\odot$. Given the small Einstein radius, microlensing event rate caused by a central IMBH in Galactic GCs strongly depends on the surface density of background sources. A region with crowded background star will greatly enhance the probability of microlensing events to occur, making GCs located in Galactic Center region viable candidates.

Accordingly, a quantitative determination of the background star density for each GC is a necessary step. This work therefore performs a cluster by cluster calculation of the background star density to identify early GCs that would offer high likelihood of detectable microlensing signals.

CLUSTERS SELECTION PROCESS

GCs considered in this study are selected based on physically motivated criteria relevant to their likelihood of hosting a central IMBH and their suitability for microlensing detection. We restrict the sample by spatially selecting GCs located in the direction of the Galactic center, where the surface density of background stars is highest, thereby significantly enhancing the probability of detecting microlensing events [10].

This work was driven to adopt an alternative perspective by emphasizing physically motivated criteria in the initial selection process. By doing so, we aim to identify clusters that are intrinsically more likely to host central IMBHs, independent of observational limitations. The feasibility of detecting microlensing signals is then evaluated in a subsequent step through the background stellar density in each cluster field.

The selection is further constrained using intrinsic GCs properties. Only clusters with masses greater that $10^5\ M_\odot$ are included, as theoretical studies suggest that such systems are more likely to form and retain central IMBHs [21]. The referred study also stated that GCs with metallicity of $[Fe/H] < -1$ indicating that low metallicity environments are favorable for IMBH formation. We also consider the central velocity dispersion, selecting clusters within the range of σ_0 values approximately 10-20 km s^{-1}, as this parameter reflects the dynamical conditions required for IMBH presence and influences the microlensing signal.

Referenced values for the important parameters for GCs then shown in TABLE 1, which contains information regarding position, mass, core radius in arcminutes, central velocity dispersion, and metallicity of each GCs. The catalogued GCs are all located in the direction of the Galactic center, confirmed by the work in [20]. We referenced the value of mass and central velocity dispersion from [22] and metallicity from this catalogue [25]. Although GCs radius is not a parameter essential for the selection process, it is a crucial parameter needed for the later background star density estimation step, as it will be used to retrieve Gaia DR3 archival data. Thus, we also showed GCs radius in TABLE 1 with values referenced from the SIMBAD

TABLE 1. GCs candidates located in the direction of the Galactic center were selected based on the catalog provided by [20]. This table presents key parameters for each GCs, including mass, distance, radius, central velocity dispersion, and metallicity. Except for distance and radius, these parameters serve as the primary criteria for the cluster selection process. The asterisk symbol denotes the selected GCs.

Cluster	$\alpha(^\circ)$	$\delta(^\circ)$	$M(M_\odot)$	d (kpc)	r_c (arcmin)	σ_0 (km s^{-1})	[Fe/H]
NGC 6144	246.80875	-26.024722	4.6×10^4	8.9	9.3	2.2	-1.76
Terzan 3	247.16700	-35.353472	5.4×10^4	8.2	10.8	2.4	-0.74
NGC 6171	248.13292	-13.053056	8.7×10^4	6.4	10.0	4.3	-1.02
ESO452-SC11	249.90833	-28.399167	1.0×10^4	8.3	4.8	1.6	-1.50
NGC 6256	254.88583	-37.121389	7.2×10^4	10.3	1.7	4.5	-1.02
*NGC 6266	255.30333	-30.113611	7.0×10^5	6.8	14.1	15.2	-1.18
*NGC 6273	255.65542	-26.267500	6.8×10^5	8.8	9.6	11.0	-1.74
NGC 6293	257.54333	-26.581111	1.8×10^5	9.5	7.9	7.5	-1.99
NGC 6304	258.63438	-29.462028	2.7×10^5	5.9	6.8	5.7	-0.45
NGC 6316	259.15592	-28.140000	3.7×10^5	10.4	1.7	9.0	-0.45
NGC 6325	259.49708	-23.766111	6.2×10^4	7.8	4.3	5.9	-1.25
NGC 6342	260.29208	-19.587500	4.6×10^4	8.5	3.0	4.5	-0.55
NGC 6355	260.99417	-26.353333	3.7×10^5	5.4	5.4	6.2	-1.37
Terzan 2	261.08458	-30.761111	8.0×10^4	7.5	2.0	4.1	-0.69
Terzan 4	262.66250	-31.599444	1.8×10^5	7.2	2.0	6.2	-1.41
BH 229	262.77167	-29.981667	1.4×10^5	2.1	2.0	5.3	-1.00
Liller 1	263.35208	-33.388889	6.6×10^5	8.2	2.0	23.2	-0.33
NGC 6380	263.61667	-39.069167	3.4×10^4	10.9	3.6	8.5	-0.75
Terzan 1	263.94917	-30.469722	2.2×10^5	6.7	2.0	7.8	-1.03
Pismis 26	264.05000	-38.550000	4.3×10^4	8.2	3.0	-	-0.70
NGC 6388	264.07275	-44.735650	1.0×10^6	9.9	11.4	18.2	-0.55
NGC 6401	264.65388	-23.908750	1.2×10^5	106	9.0	6.4	-1.02
Pal 6	265.92583	-26.222500	8.6×10^4	5.8	2.0	5.4	-0.91
Terzan 5	267.02083	-24.780000	5.6×10^5	6.9	2.8	19.0	-0.23
NGC 6440	267.21946	-20.359583	4.4×10^5	8.5	4.8	15.8	-0.36
Terzan 6	267.69521	-31.274833	1.1×10^5	6.8	0.6	8.7	-0.56
NGC 6453	267.71546	-34.599889	1.6×10^5	11.6	3.0	7.6	-1.50
Terzan 9	270.41167	-26.839722	1.4×10^5	7.1	2.0	8.3	-1.05
NGC 6522	270.89200	-30.033972	3.9×10^5	7.7	5.6	8.2	-1.34
NGC 6528	271.20671	-30.055778	8.9×10^4	7.9	2.4	6.4	-0.11
NGC 6539	271.20708	-7.585861	2.5×10^5	7.8	4.8	5.9	-0.63
NGC 6540	271.53583	-27.765278	5.6×10^4	5.3	2.0	4.2	-1.35
NGC 6553	272.31533	-25.907750	2.3×10^5	6.0	10.8	8.5	-0.18
NGC 6558	272.57667	-31.763611	2.9×10^4	7.4	3.7	3.5	-1.32
NGC 6569	273.41167	-31.826667	3.0×10^5	10.9	3.6	7.5	-0.76
NGC 6624	275.91875	-30.360833	8.7×10^4	7.9	5.9	6.1	-0.44
*NGC 6626	276.13708	-24.869722	3.6×10^5	5.5	11.2	12.6	-1.32
NGC 6638	277.73417	-25.495833	1.2×10^5	9.4	3.0	6.1	-0.95
NGC 6637	277.84625	-32.348056	1.3×10^5	8.8	7.1	6.5	-0.64
NGC 6642	277.97625	-23.475833	8.7×10^4	8.1	3.0	6.9	-1.26
NGC 6652	278.94050	-32.991444	4.1×10^4	10.0	3.5	5.1	-0.81
NGC 6656	279.09975	-23.904750	4.1×10^5	3.2	24.0	8.4	-1.70
NGC 6717	283.77517	-22.701472	2.6×10^4	7.1	3.9	3.2	-1.02
NGC 6723	284.88813	-36.632250	1.5×10^5	8.7	11.0	5.3	-1.10

data archive. GCs that does not have radius data in SIMBAD are assumed to have radius within 2 arcminutes.

As shown in TABLE 1, a total of 44 GCs are initially selected based on the positional constraint. It is also shown in the TABLE 1 how the combined application of constraints on mass, central velocity dispersion, and metallicity yields a highly restrictive outcome. Of the 44 GCs; 25 fulfill the mass criterion of $M > 10^5\ M_{\odot}$, 21 GCs meet the metallicity criterion of $[Fe/H] < 0.1$, and only 6 GCs passed the central velocity dispersion criterion. When all three constraints are applied simultaneously, the passed GCs, denoted by asterisk symbols in the TABLE 1, are reduced to just three: NGC 6266, NGC 6273, and NGC 6626.

The comparatively small number of clusters satisfying the velocity dispersion constraint indicates that this parameter is the most restrictive among the three. This parameter reflects on the GCs dynamical state, so that while mass and metallicity provide necessary conditions for IMBH formation, only a limited number of clusters exhibit the required internal kinematic properties to maintain the existence of a central IMBH.

When compared to the GCs selected based on observational properties in [10], there is only one common GC between these two results in which it is NGC 6626. Consequently, this result shows that GCs with observationally favorable conditions are not necessarily those that satisfy dynamical conditions for IMBH existence. The other approach of interpretation about this result can also be seen as a combined result between observational and physical constraints may provide a more directed framework for identifying promising targets for IMBHs microlensing searches in GCs.

BACKGROUND STAR DENSITY CALCULATION

Further analysis to do is the calculation of background star density for each selected GCs. The data used in this step are obtained from Gaia DR3 archive. Gaia is a dedicated survey telescope designed to perform astrometric measurements of stars in the Milky Way. In DR3, Gaia offers an angular resolution of 0.4 arcseconds, meaning it can distinguish two stars separated by 0.4 arcseconds. Gaia also capable of observing stars with visual magnitudes in the G-band down to approximately $m_G \sim 20$.

Stellar data are retrieved using the search feature, with object name-based queries. In this step, only the three selected clusters (NGC 6266, NGC 6273, and NGC 6626) are considered, following the application of the selection criteria described in the previous section. The radius of the search circle is determined by the radius of each cluster, provided in SIMBAD data archive. Then, the retrieved data from GAIA includes right ascencion α, declination δ, parallax p, proper motion in right ascension μ_α, proper motion in declination μ_δ, and mean magnitude in G band m_G, all include their respective errors. We also ruled out stars with re-normalized unit weight error > 1.25, so we can obtain reliable measured astrometric parameters of single stars.

Not every single star in the dataset has measured proper motion values. Therefore, we filter out stars lacking proper motion measurements and compute the ratio between the number of

stars with valid proper motion value and the total number of retrieved stars. This ratio, a, is as such

$$\mathrm{a} = \frac{N_{\mathrm{star},\mu}}{N_{\mathrm{star,total}}}, \tag{7}$$

introduced as a relative completeness factor for each cluster field. This value does not represent the true Gaia completeness, but rather an empirical value that can be used as a factor to represent effective data across different GCs.

We further ruled out stars with apparent magnitude in Gaia G-band of $m_G \geq 20$. This threshold separates between relatively bright stars and faint ones, for which Gaia measurements become increasingly uncertain and less reliable. We then have datasets consisting of stars with well-measured proper motions. Cluster member stars are then separated from background stars based on their proper motion values. Each globular cluster has a characteristic proper motion, as listed in [24] and SIMBAD catalog. Thus, a two-dimensional Gaussian model was performed to distinguish between cluster members and background stars.This selection is further refined using parallax, by retaining only stars with values consistent with the cluster distance. The identified cluster stars then ruled out from the sample, and the remaining background stars are used to estimate the background stellar density of bright stars, s_{bright}, using this equation

$$s_{\mathrm{bright}} = \frac{N_{\mathrm{bright}}}{Area\ (\mathrm{arcsec}^2)}. \tag{8}$$

To maximize the probability of detecting microlensing events caused by a central IMBHs in GCs, we also need to estimate the background star density in the faint-magnitude regime. This is important because microlensing can temporarily magnify undetectable faint stars above the magnitude threshold. In other words, stars that are too dim to be observed in their unlicensed state may become detectable during a microlensing event, so the contribution of faint background sources must be included in the analysis.

At this calculation stage, we compare our Gaia based results with the approach of [10]. In the referenced work, the background star density was derived from HST data. They scaled out the density of bright stars of each eight GCs to the SWEEP field data. We adopt this provided value as the reference background star density in faint region, denoted as s_{dim}. A scaling factor is then defined to relate between s_{bright} and s_{dim} such as

$$\text{scaling factor} = \frac{s_{\mathrm{bright}}}{s_{\mathrm{dim}}}. \tag{9}$$

The values of Gaia based s_{bright} for the eight reference clusters (47 Tucanae, NGC 362, M4, NGC 6304, NGC 6528, NGC 6553, M28, and M22) are estimated by applying the selection procedure described above to each of GCs fields.

FIGURE 1 shows the proper motion distribution of stars in the field of eight reference GCs in (μ_α, μ_δ) plane. The red points represent stars identified as cluster members, while the green points correspond to background stars. The cluster members form a compact and well-defined

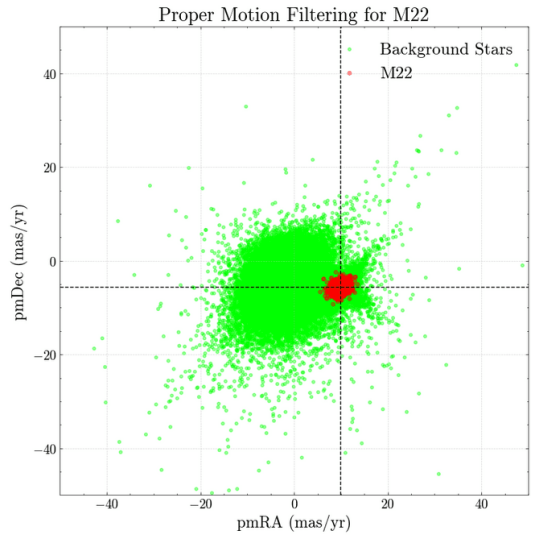
Proper Motion Filtering for M22
Background Stars
M22
pmDec (mas/yr)
pmRA (mas/yr)

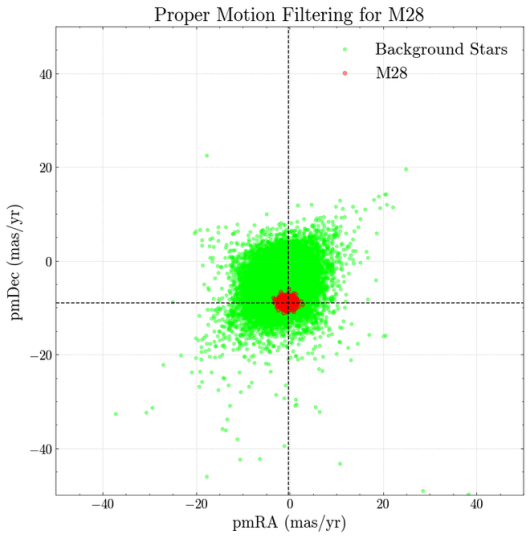
Proper Motion Filtering for M28
Background Stars
M28
pmDec (mas/yr)
pmRA (mas/yr)

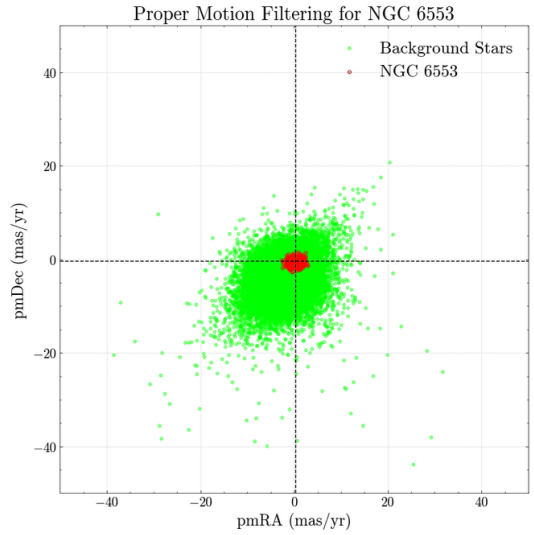
Proper Motion Filtering for NGC 6553
Background Stars
NGC 6553
pmDec (mas/yr)
pmRA (mas/yr)

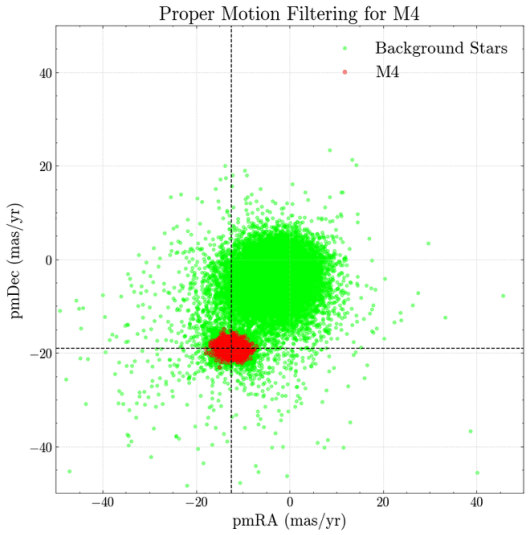
Proper Motion Filtering for M4
Background Stars
M4
pmDec (mas/yr)
pmRA (mas/yr)

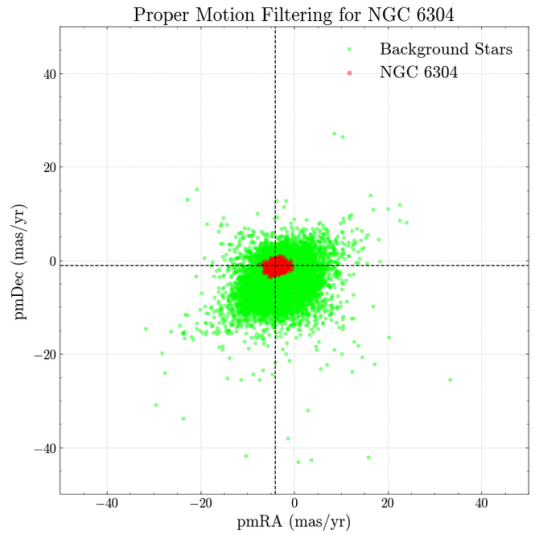
Proper Motion Filtering for NGC 6304
Background Stars
NGC 6304
pmDec (mas/yr)
pmRA (mas/yr)

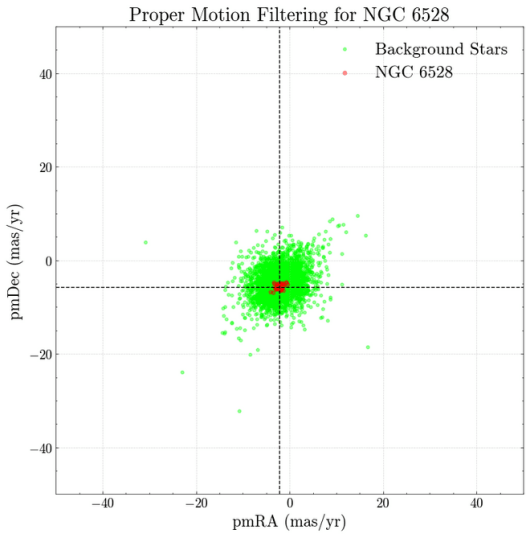
Proper Motion Filtering for NGC 6528
Background Stars
NGC 6528
pmDec (mas/yr)
pmRA (mas/yr)

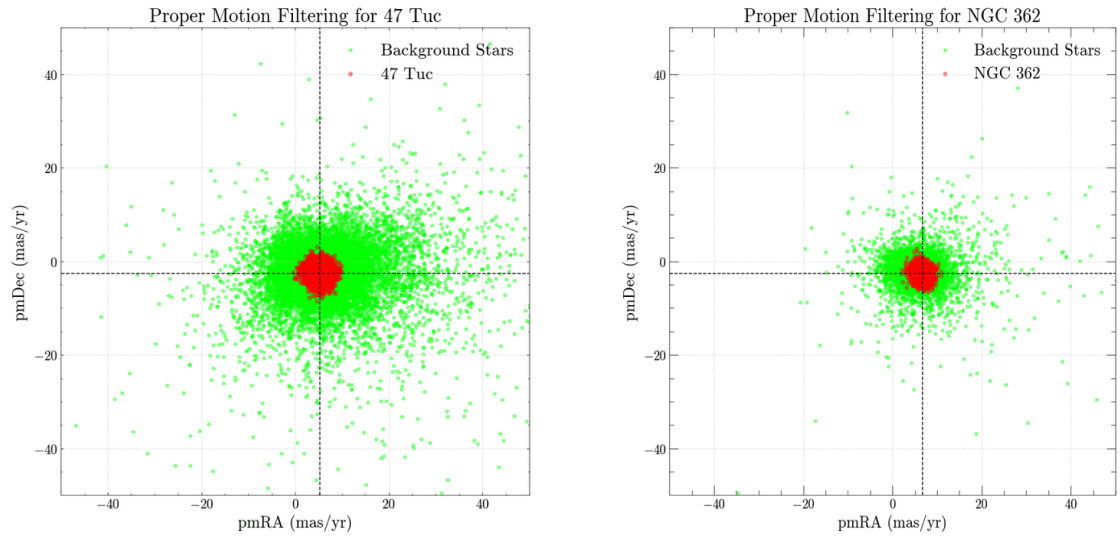

FIGURE 1. Proper motion filtering process done on eight reference GCs. Six of the GCs are located at the direction of galactic bulge (M4, NGC 6304, NGC 6528, NGC 6553, M28, and M22) and two are located at the direction of Small Magellanic Cloud (47 Tucanae and NGC 362). Cluster member stars are identified by red and background stars are identified by blue. This figure shows that most of the star retrieved from GAIA data are background stars.

kinematic properties. In contrast, background stars exhibit a much broader and more dispersed distribution, indicating a mixture of stellar populations. In this step, the processed dataset consist only of background stars since cluster member stars are removed, so it can be used directly to estimate s_{bright} for each cluster.

After carrying out the calculation, the Gaia based relative completeness factor (a), Gaia based s_{bright}, and HST based s_{dim} for each referenced GCs are then shown in TABLE 2, which also consists of astrometric parameters of the GCs (μ_α, μ_δ and parallax) and calculated scaling factor.

Based on TABLE 2, we further investigate whether the values of scaling factor are associated with the relative completeness factor. We perform a non-parametric analysis between these two parameters using the Leave-One-Out validation and Theil-Sen Regression. These methods are selected considering the small sample, and the distribution is hard to assume to be

TABLE 2. s_{dim} of reference GCs calculated based on scaling factor obtained from equation (10) based on LOO and from EQUATION (11) based on Theil-Sen regression. Based on the calculation, s_{dim} obtained from Theil-Sen regression had close values with referenced values from [10].

Cluster	a (%)	*scaling factor*		s_{bright}	$s_{\text{dim,LOO}}$	$s_{\text{dim,Theil-Sen}}$	$s_{\text{dim,Kains}}$
		LOO	Theil-Sen				
M4	79.47	0.263	0.083	0.008	0.03	0.09	0.10
NGC 6304	52.07	0.097	0.022	0.098	1.00	4.28	0.35
NGC 6528	55.14	0.057	0.029	0.091	1.57	3.07	3.20
NGC 6553	59.24	0.0001	0.050	0.079	485.85	1.58	1.60
M28	63.26	0.050	0.052	0.078	1.54	1.50	1.50
M22	69.11	0.124	0.151	0.196	1.57	1.29	1.20
47 Tucanae	82.51	0.292	0.089	0.006	0.02	006	0.02
NGC 362	73.32	0.174	0.069	0.009	0.05	0.12	0.09

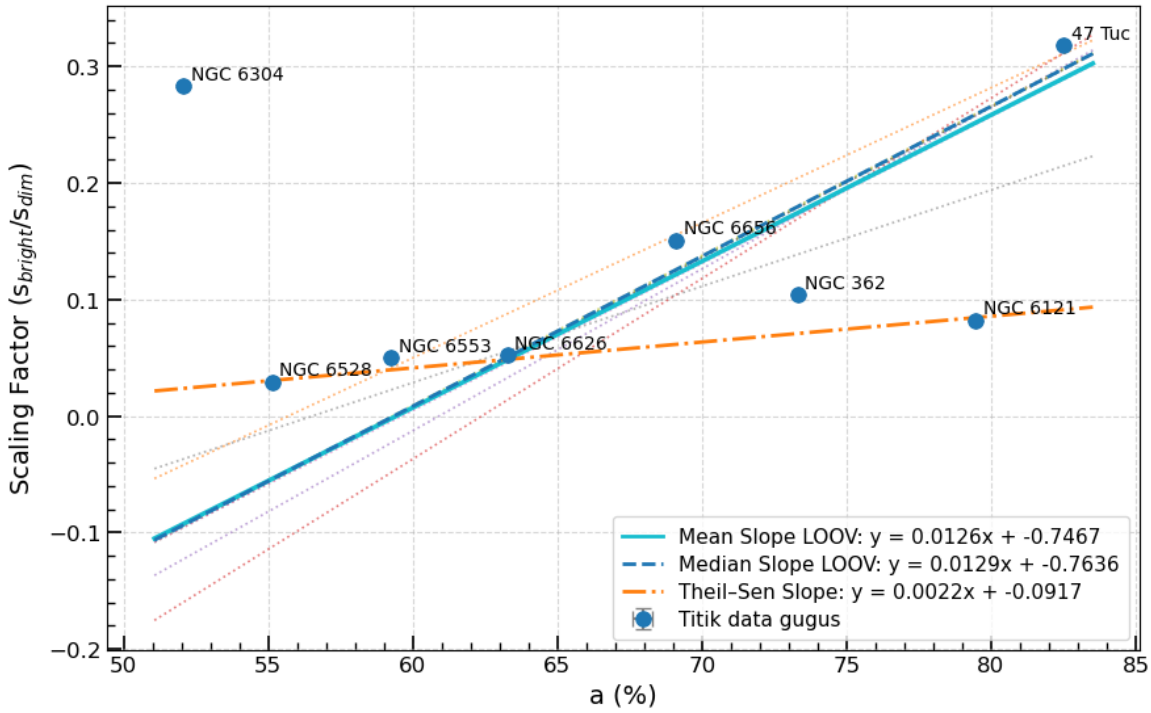

FIGURE 2. The ratio of number of stars with proper motion data to number of total stars data, a, were empirically influenced the scaling factor value, based on s_{bright} calculation done on reference GCs. Leave-One-Out validation and Theil-Sen Regression was performed to derive the correction factor between scaling factor and a value. This correction factor will be used in s_dim calculation for selected GCs.

Gaussian. In this sense, the analysis is used as an empirical comparison between the two parameters.

As shown in FIGURE 2, the fitting result obtained using the Leave-One-Out (LOO) validation method yields a steeper gradient compared to the Theil–Sen estimator. The relation derived from the LOO fitting is given by

$$\text{scaling factor}_{\text{LOO}} = 0.0128\text{a} - 0.7636, \tag{10}$$

while the Theil–Sen estimator provides the relation

$$\text{scaling factor}_{\text{Theil-Sen}} = 0.0022\text{a} - 0.0917. \tag{11}$$

Both relations are subsequently used to compute s_{dim} for each reference cluster to check which one produces more accurate results, and the results are compared in TABLE 3. As shown in the table, the scaling factor obtained from the Theil–Sen estimator produces s_{dim} values that

TABLE 3. s_{bright} and s_{dim} calculated from Gaia data on selected GCs. The reference GCs that also selected are marked with *, since s_{dim} of them is known.

Cluster	μ_α	μ_δ	p	radius (arcmin)	a (%)	s_{bright}	s_{dim}	*scaling factor*
NGC 6266	-4.99	-2.95	0.185	14.1	62.953	0.347	3.86	0.090
NGC 6273	-3.23	1.66	0.142	9.6	68.172	0.197	2.18	0.091
NGC 6626	-0.27	-8.92	0.200	11.2	63.268	0.078	1.54	0.052

are generally closer to the reference values for most clusters, with the exception of NGC 6304 and 47 Tucanae. This discrepancy is likely due to the fact that, in the Theil–Sen estimation, several data points, namely NGC 6304, NGC 6656, NGC 362, and 47 Tucanae [26], are treated as outliers. Based on these results, the scaling factor and corresponding s_{dim} values used in subsequent calculations are those derived from the Theil–Sen estimator.

Afterward, we carry out calculation of s_{dim} for each of the three selected GCs. As explained before, background stars are separated from cluster stars by their proper motion, which is identified by characteristic proper motion of the GCs, as shown in FIGURE 3. The resulting background field star sample is then used to estimate s_{dim} for each selected cluster.

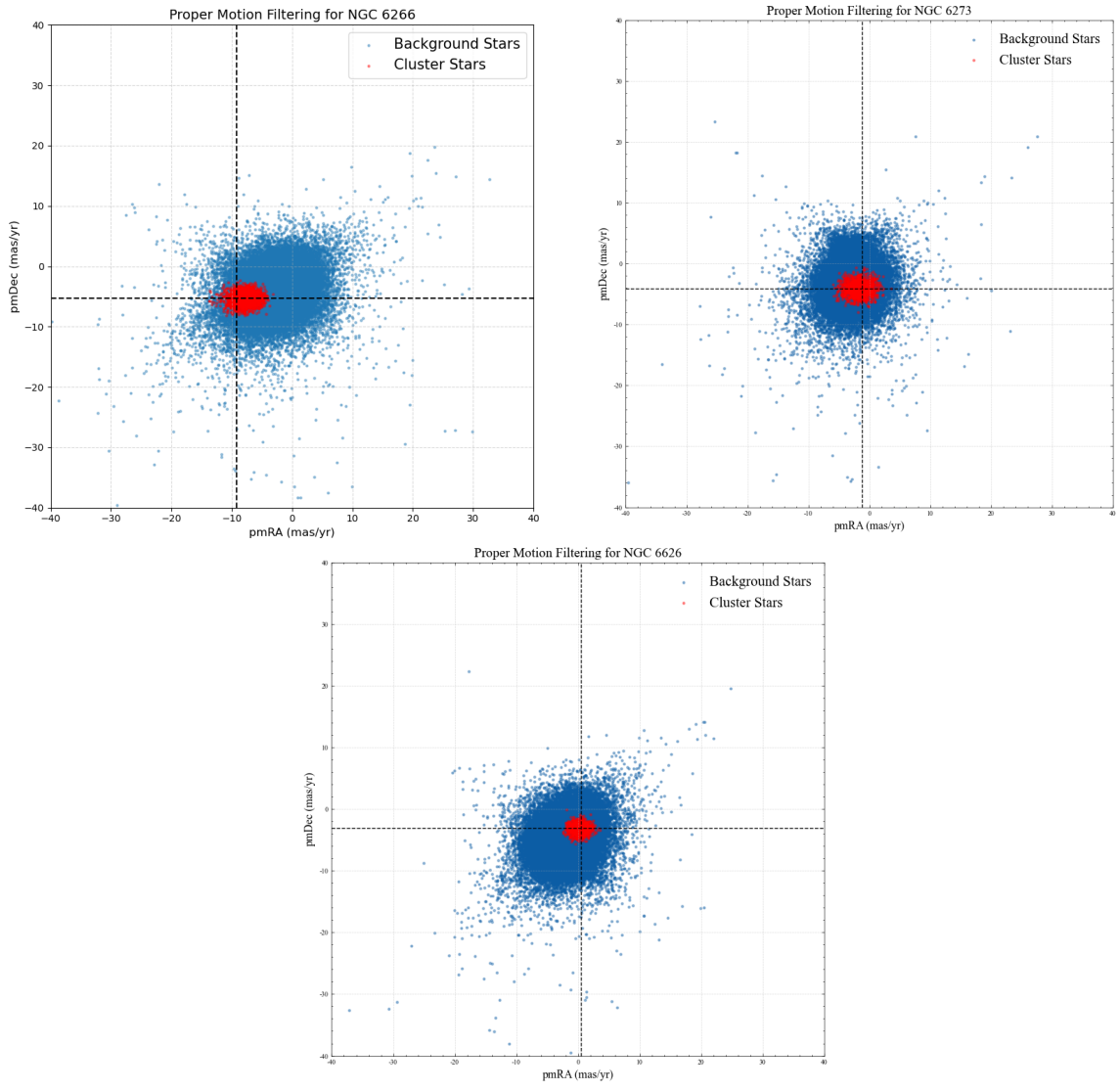

FIGURE 3. Proper motion filtering process done on three selected GCs. Cluster member stars are identified by red and background stars are identified by blue. This figure shows that most of the star retrieved from Gaia data are background stars.

TABLE 3 provides results and all the parameters used in this step of calculation. We the calculate for selected GCs using the same method used to calculate for reference GCs. After that, we calculate using EQUATION (10). FIGURE 4 shows proper motion filtering results for each selected GCs, and TABLE 3 provides the results of the calculation.

SUMMARY

In this work, we carried out literature studies and selection step of GCs located toward the direction of the Galactic center, based on physical criteria including mass, metallicity, and central velocity dispersion. These parameters were chosen to identify GCs that are intrinsically favorable for hosting a central IMBHs. The combined application of these constraints resulted in a highly restrictive selection, in which only three GCs passed all the constraints: NGC 6266, NGC 6723, and NGC 6626. This outcome highlights the strong filtering effect of the adopted criteria, particularly the central velocity dispersion, which significantly limits the number of candidates. Notably, NGC 6626 is also included in the sample identified by the referenced work [13], providing a point of consistency between the physical-motivated selection in this work and the observational-driven approach adopted in the reference study.

Following the selection process, we then estimated the background stellar density for each cluster by utilizing Gaia DR3 data. The bright-star density, s_{bright}, was derived from filtered Gaia data, while the faint-star density, s_{dim}, was estimated using a scaling factor derived from empirical calibration between reference s_{dim} values from [10] and obtained s_{bright} from Gaia data. The resulting background star densities for each GCs are summarized in TABLE 4. These values provide an essential input for evaluating the detectability of microlensing events in each GCs field.

It is important to note that this analysis is subject to several limitations. The scaling relation between s_{bright} and s_{dim} is empirical and based on a limited number of reference clusters, which may introduce uncertainties in the derived densities. In addition, the relative completeness factor used in this work does not fully represent the true observational completeness of Gaia data, which would require detailed simulations. Therefore, the estimated background densities should be interpreted as approximate indicators rather than precise measurements.

Despite these limitations, the present study provides a physically motivated and systematically derived set of GC candidates for IMBH microlensing detection searches. The identification of NGC 6266, NGC 6273, and NGC 6626 as promising targets offers a focused sample for further investigation. The next step of this work will involve performing Monte Carlo microlensing simulations to quantify the detection probability of IMBH-induced lensing events in these clusters. This will enable a more rigorous assessment of their potential as observational targets and further refine the selection strategy for future studies.

ACKNOWLEDGEMENT

This work presents results from the European Space Agency (ESA) space mission Gaia. Gaia data are being processed by the Gaia Data Processing and Analysis Consortium (DPAC). Funding for the DPAC is provided by national institutions, in particular the institutions participating in the Gaia MultiLateral Agreement (MLA). The Gaia mission website is https://www.cosmos.esa.int/gaia. The Gaia archive website is https://archives.esac.esa.int/gaia.

We also acknowledge the support of the Program Penelitian, Pengabdian Masyarakat, dan Inovasi (PPMI) ITB 2025 No. 5T/IT1.C02/KU/2025 for this research.

REFERENCES

[1] J. E. Greene, J. Strader, and L. C. Ho, "Intermediate-Mass Black Holes," *Annual Review of Astronomy and Astrophysics,* vol. 58, pp. 257–312, 2020, doi: 10.1146/annurev-astro-032620-021835

[2] A. Heger and S. E. Woosley, "The Nucleosynthesis Signature of Population III," *The Astrophysical Journal*, vol. 567, pp. 532–543, 2002, doi: 10.1086/338487

[3] B. Paczyński, "Gravitational Microlensing by the Galactic Halo," *The Astrophysical Journal*, vol. 304, pp. 1-5, 1986, doi: 10.1086/164140

[4] R. A. Remillard and J. E. McClintock, "X-Ray Properties of Black-Hole Binaries," *Annual Review of Astronomy and Astrophysics*, vol. 44, pp. 49–92, 2006, doi: 10.1146/annurev.astro.44.051905.092532

[5] W. R. Brown, "Hypervelocity Stars," *Annual Review of Astronomy and Astrophysics*, vol. 53, pp. 15–49, 2015, doi: 10.1146/annurev-astro-082214-122230

[6] Event Horizon Telescope Collaboration, K. Akiyama, A. Alberdi, et al., "First Sagittarius A* Event Horizon Telescope Results. I. The Shadow of the Supermassive Black Hole in the Center of the Milky Way," *The Astrophysical Journal Letters*, vol. 930, 2, p. L12, 2022, doi: 10.3847/2041-8213/ac6674

[7] M. J. Rees, "Black Hole Models for Active Galactic Nuclei," *Annual Review of Astronomy and Astrophysics,* vol. 22, pp. 471–506, 1984, doi: 10.1146/annurev.aa.22.090184.002351

[8] J. F. W. Baggen, P. van Dokkum, I. Labbé, et al., "Sizes and Mass Profiles of Candidate Massive Galaxies Discovered by JWST at $7 < z < 9$: Evidence for Very Early Formation of the Central 100 pc of Present-day Ellipticals," *The Astrophysical Journal Letters*, vol. 955, 1, p. L12, 2023, doi: 10.3847/2041-8213/acf5ef

[9] E. Vasiliev and H. Baumgardt, "Gaia EDR-3 View on Galactic Globular Clusters," *Monthly Notices of the Royal Astronomical Society*, vol. 505 4, pp. 5978–6002, 2021, doi: 10.1093/mnras/stab1475

[10] N. Kains, D. M. Bramich, K. C. Sahu, and A. Calamida, "Searching for Intermediate-Mass Black Holes in Globular Clusters with Gravitational Microlensing," *Monthly Notices of the Royal Astronomical Society,* vol. 460, 2, pp. 2025–2035, 2016, doi: 10.1093/mnras/stw1137

[11] M. Volonteri, "Formation of Supermassive Black Holes," *Astronomy and Astrophysics Review*, vol. 18, 3, pp. 279–315, 2010, doi: 10.1007/s00159-010-0029-x

[12] K. Sharma and C. L. Rodriquez, "From Young Massive Clusters to Old Globular Clusters: Density Profile Evolution and Intermediate-Mass Black Hole Formation," *The Astrophysical Journal*, vol. 983, 2, id. 162, 2025, doi: 10.3847/1538-4357/adbbdf

[13] M. Dominik and K. C. Sahu, "Astrometric Microlensing of Stars," *The Astrophysical Journal*, vol. 534, 1, pp. 213–226, 2000, doi: 10.1086/308716

[14] M. Servillat, S. A. Farrell, D. Lin, et al., "X-Ray Variability and Hardness of ESO 243-49 HLX-1: Clear Evidence for Spectral State Transitions," *The Astrophysical Journal*, vol. 743, 1, pp. 1-12, 2011, doi: 10.1088/0004-637X/743/1/6

[15] S. Kamann, L. Wisotzki, M. M. Roth, et al., "The Central Dynamics of M3, M13, and M92: Stringent Limits on the Masses of Intermediate-Mass Black Holes," *Astronomy and Astrophysics*, vol. 566, A58, pp. 1-24, 2014, doi: 10.1051/0004-6361/201322183
[16] M. Mezcua, "Observational Evidence for Intermediate-Mass Black Holes," *International Journal of Modern Physics D*, vol. 26, 11, id. 1730021, 2017, doi: 10.1142/S021827181730021X
[17] H. Baumgardt, J. Makino, and P. Hut, "Which Globular Clusters Contain Intermediate-Mass Black Holes?" *The Astrophysical Journal*, vol. 620, 1, pp. 238-243, 2005, doi: 10.1086/426893
[18] N. Kains, A. Calamida, K. C. Sahu, et al., "A Search for Black Hole Microlensing Signatures in Globular Cluster NGC 6656 (M22)," *The Astrophysical Journal*, vol. 867, 1, id. 37, 2018, doi: 10.3847/1538-4357/aae311
[19] Z. Wu and L. C. Ho, "Detecting Intermediate-mass Black Holes Using Quasar Microlensing," *The Astrophysical Journal*, vol. 985, 2, id. 197, 2025, doi: 10.3847/1538-4357/adcec3
[20] A. T. Bajkova, A. A. Smirnov, and V. V. Bobylev, "Analysis of Orbital Dynamics of Globular Clusters in the Central Region of the Milky Way," *Astrophysical Bulletin*, vol. 80, pp. 369–393, 2025, doi: 10.1134/S1990341325600310
[21] M. S. Fujii, L. Wang, A. Tanikawa, et al., "Simulations Predict Intermediate-Mass Black Hole Formation in Globular Clusters," *Science*, vol. 384, 6703, pp. 1488–1492, 2024, doi: 10.1126/science.adi4211
[22] H. Baumgardt and M. Hilker, "A Catalogue of Masses, Structural Velocity Dispersion Profiles of 112 Milky Way Globular Clusters," *Monthly Notices of the Royal Astronomical Society*, vol. 478 2, pp. 1520–1557, 2018, doi: 10.1093/mnras/sty1057
[23] P. Schneider, J. Ehlers, E. E. Falco, "Gravitational Lenses", Berlin: *Springer*, 1992, doi: 10.1007/978-3-662-03758-4
[24] Y. Tsapras, Y., "Microlensing Searches for Exoplanets," *Geosciences*, vol. 8, 10, id. 365, 2018, doi: 10.3390/geosciences8100365
[25] W. E. Harris, "A Catalog of Parameters for Globular Clusters in the Milky Way," *The Astronomical Journal*, vol. 112, p. 1487, 1996, doi: 10.1086/118116
[26] B. Kızıltan, H. Baumgardt, and A. Loeb, "An Intermediate-Mass Black Hole in the Centre of the Globular Cluster 47 Tucanae," *Nature*, vol. 542, pp. 203–205, 2017, doi: 10.1038/nature21361